DOI: 10.1002/pssr.201800564
Article type: Full Paper

Fundamental Properties of Co-Evaporated $RbInSe_2$ Thin Films

Tim Kodalle[*]*, Ramya Kormath Madam Raghupathy, Tobias Bertram, Natalia Maticiuc, Hasan A. Yetkin, René Gunder, Rutger Schlatmann, Thomas D. Kühne, Christian A. Kaufmann, Hossein Mirhosseini*

T. Kodalle, Dr. T. Bertram, Dr. N. Maticiuc, H. A. Yetkin, R. Gunder, Prof. Dr. Schlatmann, Dr. C. A. Kaufmann
PVcomB/Helmholtz-Zentrum Berlin für Materialien und Energie, Schwarzschildstr. 3, 12489 Berlin, Germany
E-mail: tim.kodalle@helmholtz-berlin.de

Dr. R. Kormath Madam Raghupathy, Prof. Dr. T. D. Kühne, Dr. H. Mirhosseini
Dynamics of Condensed Matter and Center for Sustainable Systems Design, Chair of Theoretical Chemistry, University of Paderborn, Warburger Str. 100, 33098 Paderborn, Germany

H. A. Yetkin
Technical University Berlin, Straße des 17. Juni 135, 10623 Berlin, Germany

Prof. Dr. R. Schlatmann
Hochschule für Technik und Wirtschaft Berlin, Treskowallee 8, 10318 Berlin, Germany

Keywords: $RbInSe_2$ deposition, CIGSe thin film solar cells, electronic structure, crystal structure, defect calculation

Abstract: The formation of an Rb-containing In-Se compound at the surface of $Cu(In,Ga)Se_2$ (CIGS) thin films is assumed to be part of the mechanism of RbF post deposition treatments (PDTs) performed on these absorber layers. Alkali-PDTs have acquired attention lately as they significantly enhance the efficiency of CIGS solar cells. In this contribution we investigate the formation of various phases during the RbF-PDT. Our results indicate that $RbInSe_2$ is the most probable phase to form. Combining theoretical and experimental investigations we report fundamental properties of a thermally co-evaporated $RbInSe_2$ thin film in order to serve as reference values in further studies.

1. Introduction

In the last few years, progress of the conversion efficiencies of thin film solar cells based on $Cu(In,Ga)Se_2$ (CIGS) absorber layers was driven by post deposition treatments (PDTs) using heavy alkali metal fluorides like KF, RbF and CsF.[1-4] While the overall record efficiency was achieved by a CsF-PDT,[4] the best results for absorber layers deposited by thermal co-evaporation were reached using RbF.[3] One of the main findings in most studies investigating the mechanism behind the alkali-PDTs is that an alkali-In_xSe_y-layer forms at the surface of the CIGS absorber layer during the PDT.[5-11] Combining these experimental results with theoretical calculations lead to the hypothesis that this surface compound is an $AInSe_2$ (A= K, Rb, Cs depending on the PDT),[12] which would have a higher bandgap compared to CIGS and therefore could reduce the interface recombination velocity. In a recent publication the authors were able to prove that in case of an RbF-PDT a thin layer of $RbInSe_2$ is indeed forming at the surface of the CIGS.[13] However, still little is known about the properties of such an $AInSe_2$ compound. While there are a few reports investigating K-In_xSe_y in more detail,[14-15] so far there is no published study known to us focusing on the properties of $RbInSe_2$ thin films. Although one publication regarding the fundamental structure of an $RbInSe_2$ single crystal is available,[16] an equivalent thin-film reference is of utmost importance to be able to identify the surface layer forming during an RbF-PDT.

In this contribution we investigate the possible phases that can form during the RbF-PDT. The experimental and calculated results indicate that $RbInSe_2$ is the most probable compound to form during the RbF-PDT process. The properties of $RbInSe_2$ and the formation of native defects in this compound are studied as well. Furthermore we deposited a corresponding thin-film reference sample by thermal co-evaporation and experimentally determined its fundamental properties. Note that we do not include Ga and Cu in both the calculations and experiment, since all studies reporting the possible formation of a secondary phase at the

surface of the CIGS are showing a strong depletion of Cu and Ga.[6-11] Especially in the already mentioned study by Taguchi et al.[13] there was no trace of Cu or Ga detectable in the $RbInSe_2$-layer.

2. Results and Discussion

Three different samples have been deposited by one-step co-evaporation on different substrates each (cf. experimental section for more details): an In-Se sample, an In-Se sample with a subsequent RbF-PDT ("In-Se + RbF-PDT") and an Rb-In-Se sample. To identify the phase content of these three samples, XRD patterns are displayed in **Figure 1**. The pattern of the In-Se layer (blue solid line) matches the one of the well-known In_2Se_3-structure (space group P61).[17] Note that there are three peaks at 18.65°, 25.75° and 32.0° in the diffractogram of our In-Se sample, which are not present in γ-In_2Se_3. They can probably be attributed to small amounts of a different In-Se phase, such as In_4Se_3. These peaks are not present in samples grown without Na-diffusion barrier (see supporting information, Figure SI 1 and SI 2). However, taking into account the composition of the films as measured by XRF (see **Table 1** and Table SI 1), it can be safely assumed that all In-Se samples consist almost solely of γ-In_2Se_3.

A subsequent RbF-PDT of the In_2Se_3 layer leads to no obvious change of the diffractogram (green solid line). The diffraction pattern of the co-evaporated Rb-In-Se (red solid line), on the other hand, fits well to a monoclinic $RbInSe_2$-structure without any other phases being present. **Table 2** shows the lattice and microstructural parameters of all three structures as derived by Le Bail analysis of the measured XRD patterns.[20]

Theoretically, the presence of Rb in the In-Se system can lead to the formation of various phases. The phase diagram for the Rb-In-Se system adapted from the Materials Project

Database is shown in **Figure 2**.[21] The list of the competing phases, their calculated formation energies, and bandgaps (calculated as discussed in the methodology section) are listed in **Table 3**. Our theoretical predictions for the formation energy and bandgap of the Rb-In-Se system are in good agreement with the results of a previous study.[12] Although by the evaluation of the formation energies we cannot determine which phase is the most stable one in the In-Rb-Se system, it is helpful to compare the calculated bandgaps and atomic structures of the phases with the ones observed experimentally.

From the stability diagram (see Supplementary Information, Figure SI4) for the Rb-In-Se system, it is evident that if the chemical potentials of the constituent elements change gradually, In_2Se_3 can decompose to InSe and Se. This is not a likely reaction since the films are growing under Se-rich conditions. Another possibility is the following reaction: In_2Se_3 + Rb_2Se –> 2 $RbInSe_2$, which has a negative formation enthalpy (-1.41 *e*V) indicating it is likely to happen. Note that the formation of Rb_xSe_y phases is only possible under Se-rich and Rb-rich conditions, which are given in the deposition processes that we performed. However, no peak corresponding to the Rb_xSe_y phases is observed in the XRD patterns.

In **Figure 3** the absorption coefficients of all three samples, as derived from reflectance and transmission measurements are shown. To minimize the impact of the substrate on the optical analysis, soda lime glass without diffusion barrier has been used here. It has been verified that the effect of the substrate on the structural properties and the composition of the layer is negligible, although the presence of Na does affect the morphology of the films very slightly (see supplementary information, Figure SI 2, SI 3 and Table SI 1). By linearly fitting the slope of the leading edge of the absorption spectra, the optical bandgap E_g was derived. The optical bandgap of the main direct transition of all three thin films can be found along with the composition and layer thickness, in Table 1. The In_2Se_3 + RbF sample shows no notable change of the absorption coefficient, whereas the one of the $RbInSe_2$ film is larger compared

to In_2Se_3. The measured and calculated bandgap of our $RbInSe_2$ does not match the one of an $RbInSe_2$ single crystal calculated by Huang et al. based on XRD-measurements.[16] The authors calculated E_g using the LDA functional, which is known to underestimate the bandgap.[23] The lattice parameters derived by Huang et al. match our results, indicating that the structure of our $RbInSe_2$ thin film is similar to the one of the single crystal. The absorption coefficient of $RbInSe_2$ shows a rather strong absorption below the leading edge (see Figure 3) which might be attributed e.g. to tail states. Extrapolation of this second absorption edge gives a value of $E = (2.0 \pm 0.1)$ *e*V (dashed line in Figure 3), which fits the one obtained in the study of Huang et al.[16] Furthermore our value of $E_g = (2.8 \pm 0.1)$ *e*V is in very good agreement with the results of our theoretical prediction (see Table 3) as well as the one of another previously reported theoretical calculation.[12] However based on these results, no direct conclusion can be drawn on the formation of $RbInSe_2$ during the RbF-PDT of CIGS. Nonetheless, as a result of an earlier X-Ray Photoelectron Spectroscopy (XPS) investigation a good match of the Rb 3d core level binding energies was already shown between the same $RbInSe_2$ sample discussed here to those of RbF-treated CIGS.[24] We also investigated the formation of intrinsic defects in $RbInSe_2$. Formation energies for these defects under Se-rich conditions are shown in **Figure 4**. All intrinsic defects with low formation energies are donor-like defects, i.e. according to our calculation $RbInSe_2$ with intrinsic defects is an *n*-doped material.

The experimentally derived bandgap energy of the In_2Se_3 thin film fits well with the literature.[25] The theoretical prediction of the γ-In_2Se_3 bandgap, however, is about 0.5 *e*V larger than the measured bandgap. This might be due to an overestimation of the bandgap of structures that are optimized with the HSE functional. Independent of this issue, the measured and calculated bandgap of $RbInSe_2$ is higher than the one observed and calculated for In_2Se_3 and also higher than the one of CIGS.[26]

Incorporation of Rb into the γ-In_2Se_3 lattice can change the bandgap. We have calculated the defect formation energies for three defects in γ-In_2Se_3: two substitutional defects (Rb_{In} and Rb_{Se}) and one interstitial defect ($Rb_{i,tet}$). The formation energies for the most stable defects under Se-rich condition are shown in **Figure 5**. The interstitial defects are found to be more stable than substitutional defects for all chemical potentials of In, Se, and Rb. Moreover, the formation of substitutional and interstitial defects leads to the reduction in the bandgap energy. The formation energies of all point defects in γ-In_2Se_3 are rather high, which indicates their concentration in the system is low.

Contrary to the calculated results, the experimental incorporation of small amounts of Rb (about 0.1 at% to 0.2 at%) into In_2Se_3 has no effect on any of the experimentally investigated properties. The discrepancy between experimental and computed results could be due to the different concentration of the defects. While the experimental molar fraction of Rb is about 0.1 at%-0.2 at%, the fraction of Rb in the supercell is 4 to 8 times larger (0.8 at%).

In **Figure 6** Raman spectra of all three samples are shown. The spectrum of In_2Se_3 + RbF is almost unchanged in comparison to the one of pure In_2Se_3 indicating that the RbF-PDT did not modify the crystal structure detectable by Raman scattering, i.e. close to the surface. Just as the XRD patterns the Raman spectra of both In_2Se_3 samples fit very well to literature values for pure γ-In_2Se_3 supporting the statement that other phases are present in these layers only to a very limited amount.[15] To the best of our knowledge no Raman spectrum of an $RbInSe_2$ structure has previously been reported in the literature so far. The positions of the main peaks are indicated by markers in Figure 6. The respective error for each position is estimated to be lower than ±0.5 cm^{-1}.

Finally, **Figure 7** shows SEM images of the three different layers. In_2Se_3 and In_2Se_3 + RbF show a similar morphology consisting of small, compact grains near the back contact and

long, thin grains sticking out of this small-grained regime. The $RbInSe_2$ sample shows an overall smoother morphology with bigger grain size compared to the other two samples.

3. Conclusion

In this contribution we were able to demonstrate how to grow high-quality $RbInSe_2$ thin films by thermal co-evaporation. Due to the good agreement of the theoretical predictions and the experimentally derived properties of the $RbInSe_2$ thin film, the presented results - in particular the reported bandgap energy of about 2.8 *e*V - can be used for future reference. This might be especially of interest with respect to the interpretation of the RbF-PDTs' effect on CIGS absorber thin films.

With the methods utilized in this study we could not detect the formation of an $RbInSe_2$ phase after an RbF-PDT of an In_2Se_3 layer. However, a more surface-sensitive comparison of the chemical environment of the Rb-atoms in our $RbInSe_2$ sample with the one of an RbF-treated CIGS thin film shows good agreement.[24] The fact that both theoretical and experimental results show a higher bandgap energy for $RbInSe_2$ compared to the one of In_2Se_3 and CIGS is supporting the hypothesis that interface recombination at the CIGS/CdS junction could be reduced due to the formation of $RbInSe_2$ during an RbF-PDT. In order to validate this hypothesis, the positions of the valence band and conduction band have to be determined. Corresponding measurements are ongoing.

4. Experimental Section

The calculations presented here were performed using the Vienna Ab initio Simulation Package (VASP).[27] A plane-wave basis and projector augmented wave pseudopotentials were employed together with an energy cut off of 500 *e*V.[28, 29] The structure optimization

and electronic structure calculations were performed using the PBE generalized gradient approximation functional and Heyd-Scuserian-Ernzerhof hybrid functionals for the exchange-correlation potential, respectively.[30, 31] For the latter functional, the parameter α, which indicates the percentage of the exact exchange to be included, was modified to 0.30. It is noted that the HSE06 functional with α = 0.30 has been reported to predict the bandgaps and atomic structures of CIS, InSe and $RbInSe_2$ very close to the experimental values.[32] To sample the Brillouin zone, we used a Gamma-centered k-point mesh with a grid density of at least 500 points per number of atoms in the unit cell. The structures were considered to be optimized when the residual force on each atom was less than 0.05 *e*V $Å^{-1}$. Defect calculations were performed with the PyCDT toolkit,[33] which creates input structures for the different charged defects, whereas the defect formation energies were calculated by taking finite-size corrections into account.

For the experimental part of this study, three different thin film samples were deposited using a one-stage thermal co-evaporation process: a co-evaporated Rb-In-Se layer, an In-Se layer without any Rb and an In-Se-layer with subsequent RbF-PDT (In-Se + RbF). Soda-lime glass was used as substrate, some of which were coated with 800 nm of molybdenum. If not specified otherwise, the samples have been prepared under Na-free conditions on soda lime glass that was covered with a SiN_xO_y diffusion barrier. During the deposition processes In, Se and RbF, in case of the Rb-In-Se sample, were deposited on the substrates at a temperature of T_{Sub} = 550°C using our vacuum CIGS deposition system.[34] The temperatures of the crucibles were adjusted to reach evaporation rates of 0.4 Å s^{-1} for RbF and In each, ensuring excess Se-supply (Se-Rate approx. 1 Å s^{-1}). On one In-Se layer we performed our standard RbF-PDT (referred to as In-Se + RbF-PDT), which is described in detail elsewhere,[11] directly subsequent to the In-Se-deposition. After finishing the deposition processes all samples were

rinsed in diluted ammonia to wash off residual fluorine and excess Rb, which might be present in form of e.g. Rb_2SeO_3 or similar compounds.[11]

Grazing incidence X-Ray Diffraction (GIXRD) patterns were recorded using a PANalytical X'Pert Pro MPD diffractometer employing Cu Kα (λ = 1.54187 Å) radiation, total reflectance and total transmission were measured using a commercial UV-Vis setup by Perkin Elmer, Scanning Electron Microscopy (SEM) images were taken with a Hitachi S4100 microscope and the composition was measured by X-Ray Fluorescence spectroscopy (XRF) using a Rigaku ZSX Primus II. Raman spectra were recorded using a setup based on S&I components equipped with a laser emitting light at a wavelength of λ = 532 nm resulting in an information depth of roughly 100-150 nm. Samples grown on molybdenum were used for XRD, XRF, Raman and SEM studies, while samples grown directly on glass substrates were used for UV-Vis measurements.

Supporting Information
Supporting Information is available from the Wiley Online Library or from the author.

Acknowledgements
The authors acknowledge financial support by the German Federal Ministry for Economic Affairs and Energy in the frame of the speedCIGS project (contract numbers 0324095C, 0324095E). The authors also thank B. Bunn and K. Mayer-Stillrich for preparation of the substrates, J. Lauche and T. Münchenberg for technical support, C. Klimm for the SEM images and P. Reyes-Figueroa for fruitful discussions.

Received: ((will be filled in by the editorial staff))
Revised: ((will be filled in by the editorial staff))
Published online: ((will be filled in by the editorial staff))

References

[1] A. Chirlia, P. Reinhard, F. Pianezzi, P. Bloesch, A. R. Uhl, C. Fella, L. Kranz, D. Keller, C. Gretener, H. Hagendorfer, D. Jaeger, R. Erni, S. Nishiwaki, S. Buecheler, A. N. Tiwari, *Nature Materials* **2013**, *12*, 1107-1111.

[2] J. Nishinaga, T. Koida, S. Ishizuka, Y. Kamikawa, H. Takahashi, M. Iioka, H. Higuchi, Y. Ueno, H. Shibata, S. Niki, *Applied Physics Express* **2017**, *10*, 092301.

[3] P. Jackson, R. Wuerz, D. Hariskos, E. Lotter, W. Witte, M. Powalla, *Phys. Status Solidi RRL* **2016**, *10*, 1-4.

[4] Solar Frontier KK. Press release 20.12.2017 – URL: www.solar-frontier.com/eng/news/2017/1220_press.html

[5] P. Pistor, D. Greiner, C. A. Kaufmann, S. Brunken, M. Gorgoi, A. Steigert, W. Calvet, I. Lauermann, R. Klenk, T. Unold, M. C. Lux-Steiner, *Applied Physics Letters* **2014**, *105*, 63901.

[6] E. Handick, P. Reinhard, J. H. Alsmeier, L. Köhler, F. Pianezzi, S. Krause, M. Gorgoi, E. Ikenaga, N. Koch, R. G. Wilks, S. Buecheler, A. N. Tiwari, M. Bär, *ACS Applied Materials and Interfaces* **2015**, *7*, 27414.

[7] E. Handick, P. Reinhard, R. G. Wilks, F. Pianezzi, T. Kunze, D. Kreikemeyer-Lorenzo, L. Weinhardt, M. Blum, W. Yang, M. Gorgoi, E. Ikenaga, D. Gerlach, S. Ueda, Y. Yamashita, T. Chikyow, C. Heske, S. Buecheler, A. N. Tiwari, M. Bär, *ACS Applied Materials & Interfaces* **2017**, *9*, 3581-3589.

[8] T. Lepetit, G. Ouvrard, N. Barreau, *Prog. Photovolt: Res. Appl.* **2017**, *25*, 1068-1076.

[9] E. Avancini, R. Carron, T. P. Weiss, C. Andres, M. Bürki, C. Schreiner, R. Figi, Y. E. Romanyuk, S. Buecheler, A. N. Tiwari, *Chem. Mater.* **2017**, *29*, 9695-9704.

[10] S. Ishizuka, N. Taguchi, J. Nishinaga, Y. Kamikawa, S. Tanaka, H. Shibata, *J. Phys. Chem. C* **2018**, *122*, 3809-3817.

[11] T. Kodalle, M. D. Heinemann, D. Greiner, H. A. Yetkin, M. Klupsch, C. Li, P. A. van Aken, I. Lauermann, R. Schlatmann, C. A. Kaufmann, *Solar RRL* **2018**, *2*, 1800156.

[12] M. Malitckaya, H.-P. Komsa, V. Havu, M. J. Puska, *Journal of Physical Chemistry C* **2017**, *121*, 15516-15528.

[13] N. Taguchi, S. Tanaka, S. Ishizuka, *Appl. Phys. Lett.* **2018**, *113*, 113903.

[14] C. P. Muzzillo, L. M. Mansfield, K. Ramanathan, T. J. Anderson, *J. Mater. Sci.* **2016**, *51*, 6812-6823.

[15] T. Lepetit, S. Harel, L. Arzel, G. Ouvrard, N. Barreau, *IEEE Journal of Photovoltaics* **2016**, *6*, 1316-1320.

[16] F. Q. Huang, B. Deng, D. E. Ellis, J. A. Ibers, *J. Solid State Chem.* **2005**, *178*, 2128-2132.

[17] A. Pfitzner, H. D. Lutz, *Journal of Solid State Chemistry* **1996**, *124*, 305-308.

[18] C. Bernuy-Lopez, M. Allilx, C. A. Bridges, J. B. Claridge, M. J. Rosseinsky, *Chem. Mater.* **2007**, *19*, 1035-1043.

[19] J. H. C. Hogg, H. H. Sutherland, D. J. Williams, *Acta Crystallographica Sec. B* **1973**, *29*, 1590-1593.

[20] A. Le Bail, H. Duroy, J. L. Fourquet, *Materials Research Bulletin* **1988**, *23*, 447-452.

[21] A. Jain, S.P. Ong, G. Hautier, W. Chen, W.D. Richards, S. Dacek, S. Cholia, D. Gunter, D. Skinner, G. Ceder, K.A. Persson, *APL Materials* **2013**, *1*, 011002.

[22] D. Cahen, R. Noufi, *Journal of Physics and Chemistry of Solids* **1992**, *53*, 991-1005.

[23] J. P. Perdew, W. Yang, K. Burke, Z. Yang, E. K. U. Gross, M. Scheffler G. E. Scuseria, T. M. Henderson, I. Y. Zhang, A. Ruzsinszky, H. Peng, J. Sun, E. Trushin, A. Görling, *Proceedings of the National Academy of Sciences* **2017**, *114*, 2801–2806.

[24] N. Maticiuc, T. Kodalle, J. Lauche, R. Wenisch, T. Bertram, C. A. Kaufmann, I. Lauermann, *Thin Solid Films* **2018**, *665*, 143-147.

[25] T. Okamoto, Y. Nakada, T. Aoki, Y. Takaba, A. Yamada, M. Konagai, *Phys. Stat. Sol. C* **2006**, *3*, 2796-2799.

[26] S. Chichibu, T. Mizutani, K. Murakami, T. Shioda, T. Kurafuji, H. Nakanishi, S. Niki, P. J. Fons, A. Yamada, *Journal of Applied Physics* **1998**, *83*, 3678-3689.

[27] G. Kresse and J. Hafner, *Phys. Rev. B* **1993**, *47*, 558-561.

[28] P.E. Blöchl, *Phys. Rev. B* **1994**, *50*, 17953.

[29] G. Kresse, J. Joubert, *Phys. Rev. B* **1999**, *59*, 1758-1775.

[30] J. Heyd, G. E. Scuseria, M. Ernzerhof, *J. Chem. Phys.* **2003**, *118*, 8207-8215.

[31] J. Heyd, G. E. Scuseria, M. Ernzerhof, *J. Chem. Phys.* **2006**, *124*, 219906.

[32] S. K. Sahoo, R. Kormath Madam Raghupathy, T. D. Kühne, H. Mirhosseini, *The Journal of Physical Chemistry C* **2018**, *122*, 21202-21209.

[33] D. Broberg, B. Medasani, N. Zimmermann, A. Canning, M. Haranczyk, M. Asta, G. Hautier, *Computer Physics Comm.* **2018**, *226*, 165-179.

[34] M. D. Heinemann, R. Mainz, F. Österle, H. Rodriguez-Alvarez, D. Greiner, C. A. Kaufmann, T. Unold, *Scientific Reports* **2017**, *7*, 45463.

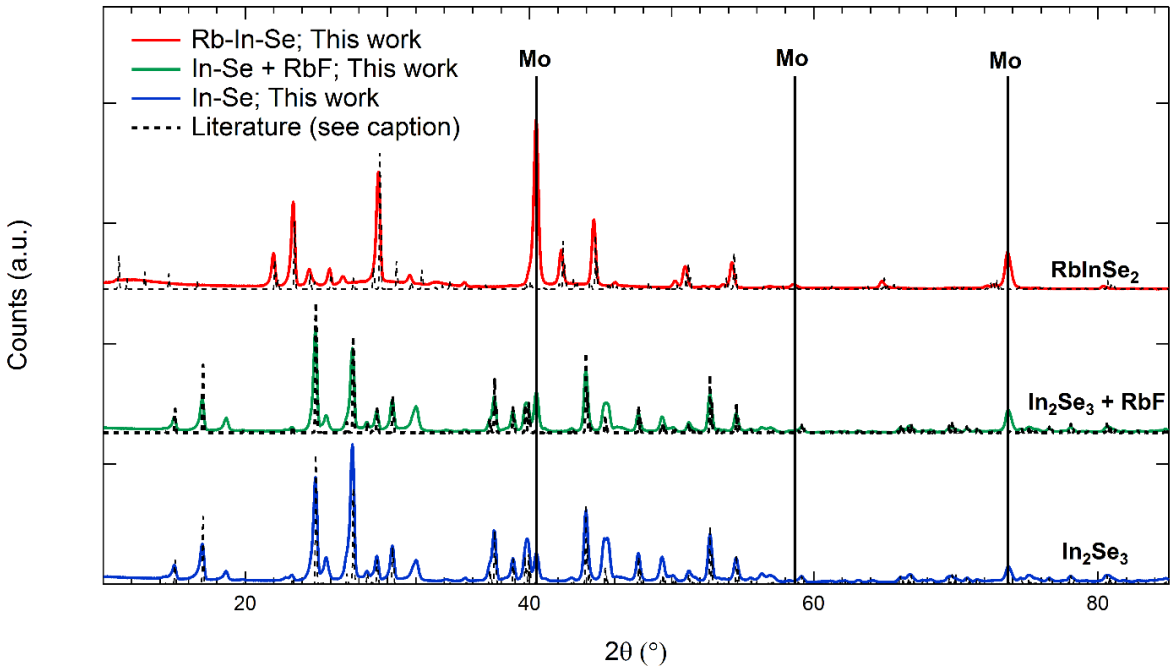

Figure 1. XRD-diffractogram of our In-Se, In-Se + RbF and Rb-In-Se samples (solid lines) in comparison to reference diffractograms of In_2Se_3 (used for In-Se and In-Se + RbF),[17] $RbInSe_2$ (dashed lines),[16] and markers showing the peaks related to the molybdenum back contact.[18]

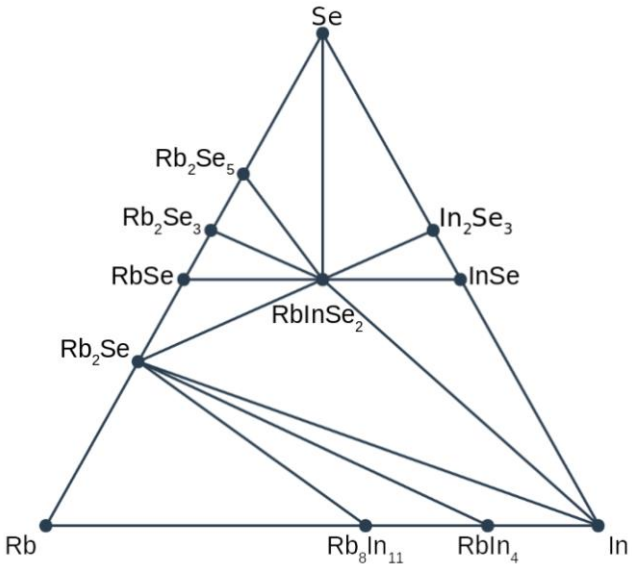

Figure 2. Phase diagram for Rb-In-Se system (adapted from Materials project database).[21]

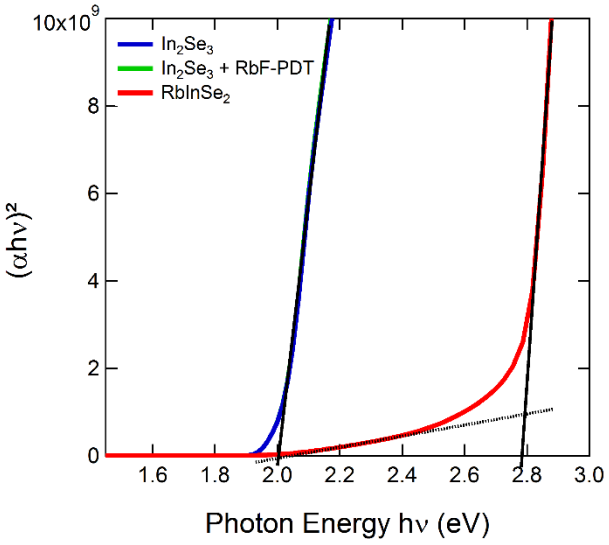

Figure 3. Determination of the bandgap of In_2Se_3, In_2Se_3 + RbF and $RbInSe_2$ thin films. The curves for In_2Se_3 and In_2Se_3 + RbF strongly overlap so that the one of In_2Se_3 + RbF is barely visible in this plot.

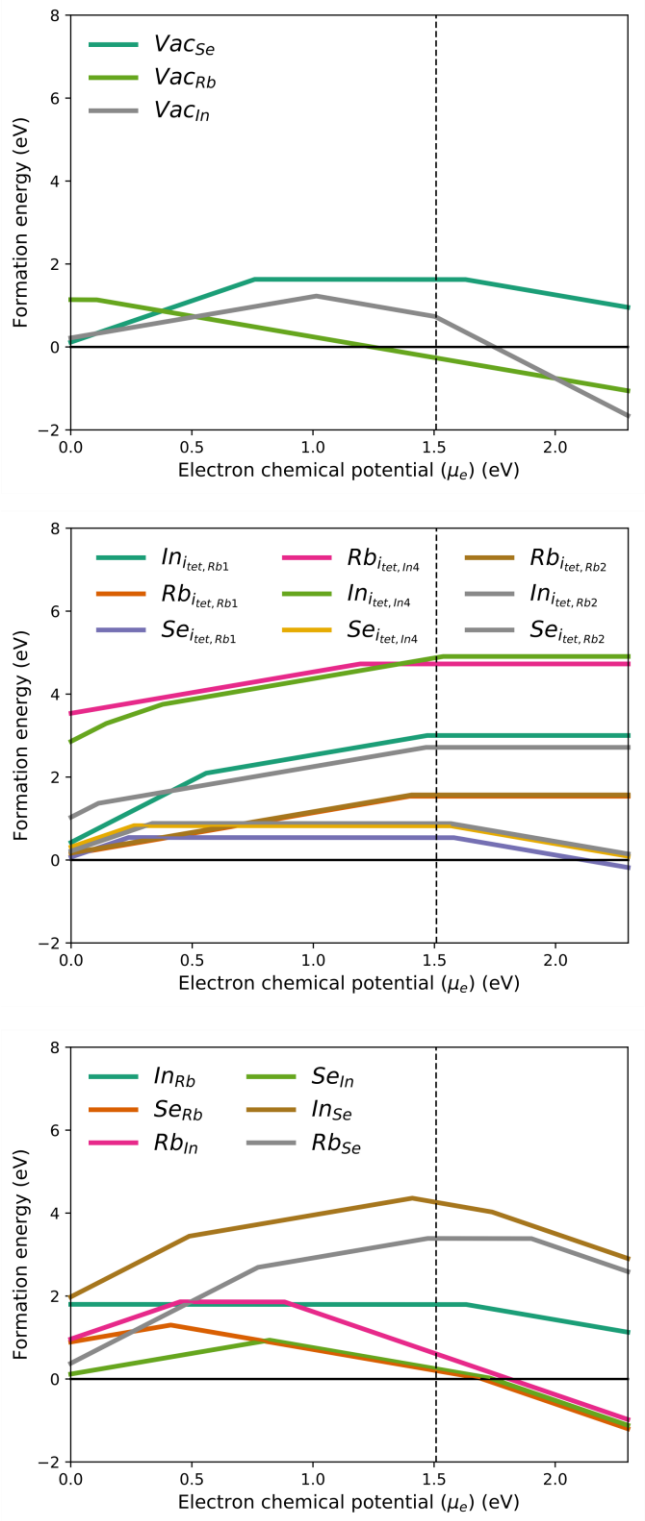

Figure 4. Defect formation energies for the $RbInSe_2$ system.

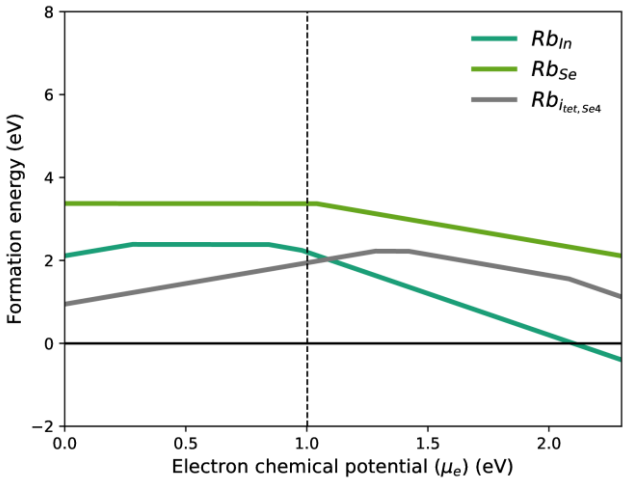

Figure 5. Defect formation energies for Rb incorporation into the γ-In_2Se_3 system.

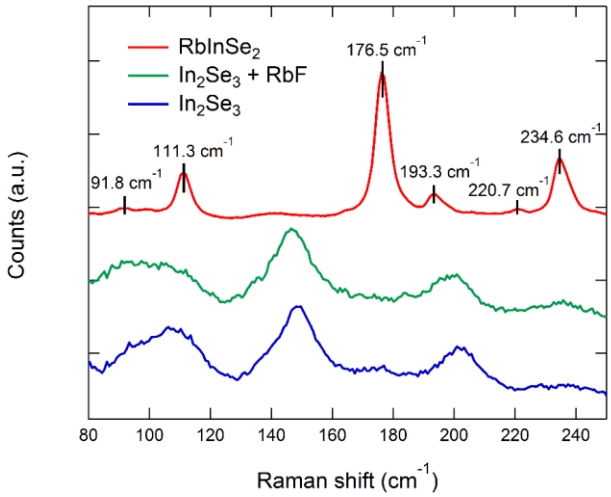

Figure 6. Raman shift of the In_2Se_3, In_2Se_3 + RbF and $RbInSe_2$ samples. The background of all three spectra was removed using an exponential function.

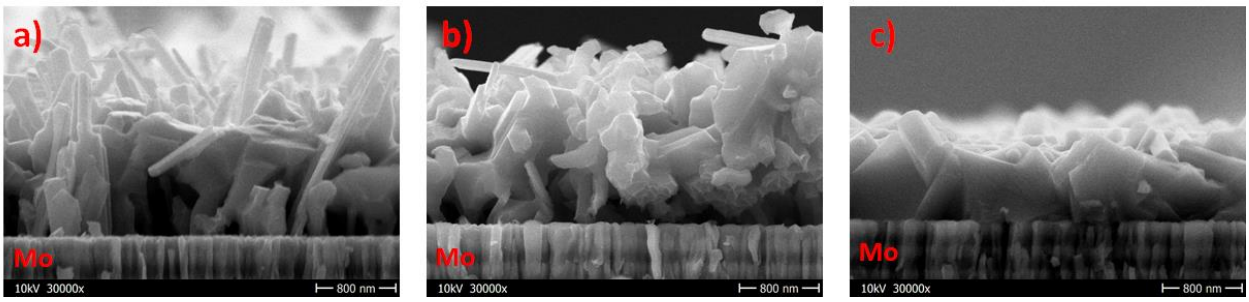

Figure 7. Cross-sectional SEM images of the In_2Se_3 (a), In_2Se_3 + RbF (b) and $RbInSe_2$ (c) samples.

Table 1. Composition of the thin films as measured by XRF after rinsing the samples in diluted ammonia. Additionally the optical bandgap of the layers as measured by UV-Vis is shown. Here χ_i denotes the molar fraction of element i.

Sample	χ_{Rb} (%)	χ_{In} (%)	χ_{Se} (%)	Thickness (nm)	E_g (eV)
In_2Se_3	0.0 ± 0.1	40.1 ± 0.1	59.9 ± 0.1	approx. 550	2.0 ± 0.1
In_2Se_3 + RbF-PDT	0.2 ± 0.1	39.9 ± 0.1	59.9 ± 0.1	approx. 550	2.0 ± 0.1
$RbInSe_2$	24.5 ± 0.1	24.4 ± 0.1	51.0 ± 0.1	approx. 800	2.8 ± 0.1

Table 2. Structural details of the three thin film samples as derived from XRD patterns.

Sample	a (Å)	b (Å)	c (Å)	β (°)	Microstrain (%)
In_2Se_3	7.124	7.124	19.393	-	0.06
In_2Se_3 + RbF-PDT	7.127	7.127	19.398	-	0.08
$RbInSe_2$	11.502	11.496	16.469	100.781	0.15

Table 3. The competing phases of the In-Se-Rb system and their formation energies and calculated bandgaps. The values in the brackets show the measured values from.[22]

Phase	Formation energy (eV)	E_g^{HSE} (eV)
γ-In_2Se_3	-3.27 (-3.57)	2.47
InSe	-1.25 (-1.22)	1.2
Rb_2Se	-3.56	3.1
Rb_2Se_3	-4.55	2.1
Rb_2Se_5	-4.67	2.2
$RbIn_4$	-0.54	-
$RbInSe_2$	-4.27	2.7
RbSe	-2.13	2.4